Analysis of Microstrip Resonators

TATSUO ITOH, SENIOR MEMBER, IEEE

Abstract—**An accurate and efficient method was developed for computing the resonant frequencies of microstrip resonators. The formulation of the problem was carried out rigorously using the full-wave analysis rather than the quasi-static approximation. The characteristic equation was derived using Galerkin's method applied in the Fourier transform domain.**

The accuracy of the method has been proven by comparing the numerical results with the experimental data. Numerical data have been provided for the microstrip resonators with different structural parameters.

Finally, the results for microstrip resonators have been used for predicting the end effect at the open end of microstrip structures.

I. INTRODUCTION

THE microstrip and disk resonators are useful integrated circuit components at microwave and millimeter-wave frequencies for building filters, oscillators, etc. [1]. The analysis of such structures, however, has been undertaken with various approximations [2]. Since the design formulas so obtained are not very accurate, the designers of such circuit components are often forced to use cut-and-try methods to obtain desired resonant characteristics. Recently, some attempts have been made to develop more rigorous methods of analysis so that better correlation between computed and experimentally obtained resonant frequency data is attained [3], [4]. These methods are, however, still based on the quasi-static approximation which is not valid at higher frequencies. Hence there is a definite need for an accurate full-wave analysis method for microstrip resonator structures. By full-wave analysis we mean the process of rigorously solving the electromagnetic (EM) boundary value problem by retaining all the field components.

In this paper, the boundary value problem associated with the microstrip resonator structure has been attacked in a rigorous manner based on the full-wave analysis. The solution of the problem has been derived using a new efficient method. Specifically, the derivation of the characteristic equation for resonant frequencies is carried out using Galerkin's technique applied in the spectral or Fourier transform domain instead of the space domain. The resonant frequencies are obtained by numerically solving the characteristic equation. The details of the analysis method will appear in Section II of this paper.

In Section III, the accuracy of the solution is demonstrated by comparing the numerical results with the experimental data. A number of numerical results are also presented for microstrip resonators with various structural parameters. In Section IV, the numerical data for microstrip resonators are used for predicting the end effect at the open end of the microstrip structures. Since the information so obtained is based on the full-wave analysis, it is believed to be useful for the design of microwave integrated circuit structures at higher frequencies at which reliability of the information on end effects derived from the conventional quasi-static approach [5]–[7] may be questionable.

Manuscript received April 3, 1974; revised June 10, 1974. This work was supported by U.S. Army Grants DA-ARO-D31-124-G77 and DA-HCO-4-74-G-0113 and by NSF Grant GK 36854.

The author is with the Electromagnetics Laboratory, Department of Electrical Engineering, University of Illinois, Urbana, Ill. 61703.

II. METHOD OF ANALYSIS

The microstrip resonator to be analyzed is shown in Fig. 1. A rectangular strip of width $2w$ and length $2l$ is placed on the substrate which is, in turn, backed by a ground plane. The sides and the top of the structure are covered with shielding walls. Thus the entire structure is considered to be the microstrip resonator located in a partially filled waveguide. It is assumed that the thickness of the strip is negligible and that all the media and conductors are lossless. The shielding waveguide and the substrate are assumed to extend to $z = \pm\infty$. For simplicity, the strip is assumed to be symmetrically located, although the present method of analysis can be easily extended to more general cases. Also, for simplicity of numerical computation and for practical consideration, the operating frequency is assumed to be below cutoff of the shielding waveguide partially filled with substrate material, although the formulation process is valid for any frequency range.

The fields existing in the structure shown in Fig. 1 are the superposition of TE (to z) and TM (to z) fields, and they can be expressed in terms of two types of scalar potentials $\phi(x,y,z)$ and $\psi(x,y,z)$. For instance,

$$E_{zi}(x,y,z) = k_i^2\phi_i + \partial^2\phi_i/\partial z^2 \tag{1a}$$

$$H_{zi}(x,y,z) = k_i^2\psi_i + \partial^2\psi_i/\partial z^2 \tag{1b}$$

$$E_{xi}(x,y,z) = \partial^2\phi_i/\partial x\,\partial z - j\omega\mu_i(\partial\psi_i/\partial y) \tag{1c}$$

$$H_{xi}(x,y,z) = j\omega\epsilon_i(\partial\phi_i/\partial y) + \partial^2\psi_i/\partial x\,\partial z \tag{1d}$$

where $i = 1, 2$ designates the substrate or the air region,

$$k_1 = (\epsilon_r\mu_r)^{1/2}k_0 \qquad k_2 = k_0 = \omega(\epsilon_0\mu_0)^{1/2}$$

$$\epsilon_1 = \epsilon_r\epsilon_0 \qquad \epsilon_2 = \epsilon_0$$

$$\mu_1 = \mu_r\mu_0 \qquad \mu_2 = \mu_0$$

ω is the operating frequency and ϵ_0 and μ_0 are the free-space permittivity and permeability, respectively.

Although it is possible to derive a set of coupled homogeneous integral equations for the boundary value problem

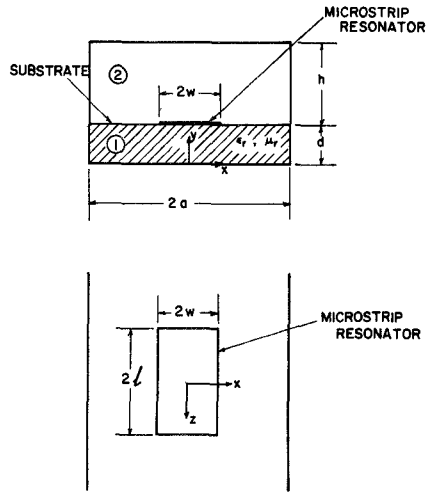

Fig. 1. End and top view of microstrip resonator.

associated with the present structure using (1) as well as all the boundary conditions, and to numerically solve these equations for the resonant frequency, this approach has been avoided in this paper. The reason is that the solution of such integral equations is numerically prohibitively difficult due mainly to the convolution integrals involving slowly convergent Green's functions. Instead, a new method is developed in which the boundary value problem associated with the structure in Fig. 1 is solved in the Fourier transform or the spectral domain. The original form of the spectral domain analysis was first developed by Itoh and Mittra and was successfully applied to a number of problems in microwave integrated circuit structures [8], [9]. The original version is extended in this paper and applied to the microstrip resonator structure. In what follows, each step to derive the characteristic equation will be described. As will be seen later, the method is numerically quite efficient.

The first step is to transform the quantities in (1) into the spectral domain via the Fourier transform:

$$\phi_i(n,y,\beta) = \int_{-\infty}^{\infty} dz \int_{-a}^{a} dx \phi_i(x,y,z) \exp(j\hat{k}_n x) \exp(j\beta z) \tag{2a}$$

$$\tilde{\psi}_i(n,y,\beta) = \int_{-\infty}^{\infty} dz \int_{-a}^{a} dx \psi_i(x,y,z) \exp(j\hat{k}_n x) \exp(j\beta z), \quad n = 1,2,\cdots \tag{2b}$$

where β is the Fourier transform variable. $\hat{k}_n$ is the discrete transform variable defined by $\hat{k}_n = (n - 1/2)\pi/a$ for E_z even $-H_z$ odd (in x) modes and $\hat{k}_n = n\pi/a$ for E_z odd $-H_z$ even (in x) modes. The transforms of field quantities are now

$$\tilde{E}_{zi}(n,y,\beta) = (k_i^2 - \beta^2)\tilde{\phi}_i \tag{3a}$$

$$\tilde{H}_{zi}(n,y,\beta) = (k_i^2 - \beta^2)\tilde{\psi}_i \tag{3b}$$

$$\tilde{E}_{xi}(n,y,\beta) = -\hat{k}_n\beta\tilde{\phi}_i - j\omega\mu_i \frac{\partial\tilde{\psi}_i}{\partial y} \tag{3c}$$

$$\tilde{H}_{xi}(n,y,\beta) = j\omega\epsilon_i \frac{\partial\tilde{\phi}_i}{\partial y} - \hat{k}_n\beta\tilde{\psi}_i. \tag{3d}$$

The transforms of scalar potentials satisfy

$$\frac{d^2}{dy^2}\tilde{\phi}_i - \gamma_i^2\tilde{\phi}_i = 0 \tag{4a}$$

$$\frac{d^2}{dy^2}\tilde{\psi}_i - \gamma_i^2\tilde{\psi}_i = 0 \tag{4b}$$

where

$$\gamma_1^2 = \hat{k}_n^2 + \beta^2 - \epsilon_r\mu_r k_0^2 \tag{5a}$$

$$\gamma_2^2 = \hat{k}_n^2 + \beta^2 - k_0^2. \tag{5b}$$

In order that $\tilde{E}_z$ and $\tilde{E}_x$ and, hence, $\tilde{E}_z$ and $\tilde{E}_x$ are zero at $y = 0$ and $y = d + h$, the solutions of (4) are

$$\tilde{\phi}_1 = A_n(\beta)\sinh\gamma_1 y \tag{6a}$$

$$\tilde{\psi}_1 = B_n(\beta)\cosh\gamma_1 y \tag{6b}$$

$$\tilde{\phi}_2 = C_n(\beta)\sinh\gamma_2(d + h - y) \tag{6c}$$

$$\tilde{\psi}_2 = D_n(\beta)\cosh\gamma_2(d + h - y) \tag{6d}$$

where A_n, B_n, C_n, and D_n are unknowns.

The second step is to apply the continuity conditions at the interface $y = d$ in the spectral domain

$$\tilde{E}_{z1}(n,d,\beta) = \tilde{E}_{z2}(n,d,\beta) \tag{7a}$$

$$\tilde{E}_{x1}(n,d,\beta) = \tilde{E}_{x2}(n,d,\beta) \tag{7b}$$

$$\tilde{H}_{z1}(n,d,\beta) - \tilde{H}_{z2}(n,d,\beta) = \tilde{J}_x(n,\beta) \tag{7c}$$

$$\tilde{H}_{x1}(n,d,\beta) - \tilde{H}_{x2}(n,d,\beta) = \tilde{J}_z(n,\beta) \tag{7d}$$

where $\tilde{J}_x(n,\beta)$ and $\tilde{J}_z(n,\beta)$ are the Fourier transforms of unknown strip-current components

$$J_x(x,z) = H_{z1}(x,d,z) - H_{z2}(x,d,z)$$

$$J_z(x,z) = H_{z1}(x,d,z) - H_{x2}(x,d,z)$$

where $|x| < w$ and $|z| < l$, and $\tilde{J}_x$ and $\tilde{J}_z$ are defined by

$$\tilde{J}_x(n,\beta) = \int_{-l}^{l} dz \int_{-w}^{w} dx J_x(x,z) \exp(j\hat{k}_n x + j\beta z) \tag{8a}$$

$$\tilde{J}_z(n,\beta) = \int_{-l}^{l} dz \int_{-w}^{w} dx J_z(x,z) \exp(j\hat{k}_n x + j\beta z). \tag{8b}$$

When (6) and (3) are substituted into (7), we obtain linear algebraic equations for unknown coefficients A_n, B_n, C_n, and D_n. When one solves these equations, the coefficients are expressed in terms of unknowns $\tilde{J}_x(n,\beta)$ and $\tilde{J}_z(n,\beta)$.

The third step is to impose the final boundary conditions

$$E_z(x,d,z) = E_x(x,d,z) = 0, \quad |x| < w, \quad |z| < l$$

in the spectral domain. To this end, let us define

$$E_z(x,d,z) = \begin{cases} 0, & |x| < w, \quad |z| < l \\ u(x,z) & \text{otherwise} \end{cases} \tag{9a}$$

$$E_x(x,d,z) = \begin{cases} 0, & |x| < w, \quad |z| < l \\ v(x,z), & \text{otherwise} \end{cases} \tag{9b}$$

where u and v are unknown. Substituting (3) and (6) into the Fourier transforms of (9), we obtain another set of algebraic relations between the transformed field quantities and unknowns A_n, B_n, C_n, and D_n. Now, A_n, B_n, C_n, and D_n are eliminated from this set of relations using the relations derived in the second step. After some mathematical manipulations, we obtain

$$\tilde{G}_{11}(n,\beta,k_0)\tilde{J}_x(n,\beta) + \tilde{G}_{12}(n,\beta,k_0)\tilde{J}_z(n,\beta) = \tilde{E}_z(n,\beta) \tag{10a}$$

$$\tilde{G}_{21}(n,\beta,k_0)\tilde{J}_x(n,\beta) + \tilde{G}_{22}(n,\beta,k_0)\tilde{J}_z(n,\beta) = \tilde{E}_x(n,\beta) \tag{10b}$$

where

$$\tilde{G}_{11} = \tilde{G}_{22} = \hat{k}_n\beta(\gamma_2 \tanh \gamma_2 h + \mu_r\gamma_1 \tanh \gamma_1 d)/\det \tag{11a}$$

$$\tilde{G}_{12} = [(\epsilon_r\mu_r k_0^2 - \beta^2)\gamma_2 \tanh\gamma_2 h + \mu_r(k_0^2 - \beta^2)\gamma_1 \cdot \tanh \gamma_1 d]/\det \tag{11b}$$

$$\tilde{G}_{21} = [(\epsilon_r\mu_r k_0^2 - \hat{k}_n^2)\gamma_2 \tanh \gamma_2 h + \mu_r(k_0^2 - \hat{k}_n^2)\gamma_1 \cdot \tanh \gamma_1 d]/\det \tag{11c}$$

$$\det = (\gamma_1 \tanh \gamma_1 d + \epsilon_r\gamma_2 \tanh \gamma_2 h)(\gamma_1 \coth \gamma_1 d + \mu_r\gamma_2 \coth \gamma_2 h) \tag{11d}$$

$$\tilde{E}_z(n,\beta) = K_z\tilde{E}_z(n,\beta) \tag{12a}$$

$$\tilde{E}_x(n,\beta) = K_x\tilde{E}_x(n,\beta). \tag{12b}$$

In (12), K_z and K_x are some known constants, while $\tilde{E}_z$ and $\tilde{E}_x$ are Fourier transforms of (9) and hence unknown. The quantities $\tilde{G}_{11}$, $\tilde{G}_{12}$, $\tilde{G}_{21}$, and $\tilde{G}_{22}$ are actually the Fourier transforms of dyadic Green's function components.

Note that (10) are algebraic equations as opposed to the coupled convolution-type integral equations which usually appear in the conventional space-domain analyses [10]. Notice also that (10) contains a total of four unknowns $\tilde{J}_x$, $\tilde{J}_z$, $\tilde{E}_x$, and $\tilde{E}_z$. However, it is possible by the application of Galerkin's procedure to eliminate the two latter unknowns $\tilde{E}_x$ and $\tilde{E}_z$ and to solve (10) for $\tilde{J}_x$ and $\tilde{J}_z$ only.

To this end, the unknowns $\tilde{J}_x$ and $\tilde{J}_z$ are first expressed in terms of known basis functions $\tilde{J}_{xm}$ and $\tilde{J}_{zm}$ with unknown coefficients c_m and d_m.

$$\tilde{J}_x(n,\beta) = \sum_{m=1}^{M} c_m\tilde{J}_{xm}(n,\beta) \tag{13a}$$

$$\tilde{J}_z(n,\beta) = \sum_{m=1}^{N} d_m\tilde{J}_{zm}(n,\beta). \tag{13b}$$

The basis functions $\tilde{J}_{xm}$ and $\tilde{J}_{zm}$ must be chosen to be the Fourier transforms of space-domain functions $J_{xm}(x,z)$ and $J_{zm}(x,z)$ which have finite support, viz., which are zero except for the region $|x| < w$ and $|z| < l$. Now, substituting (13) into (10) and taking inner products of the resulting equations with the basis functions $\tilde{J}_{xi}$ and $\tilde{J}_{zi}$ for different values of i, we obtain

$$\sum_{m=1}^{M} K_{im}^{(1,1)}c_m + \sum_{m=1}^{N} K_{im}^{(1,2)}d_m = 0, \qquad i = 1,2,\cdots,N \tag{14a}$$

$$\sum_{m=1}^{M} K_{im}^{(2,1)}c_m + \sum_{m=1}^{N} K_{im}^{(2,2)}d_m = 0, \qquad i = 1,2,\cdots,M \tag{14b}$$

where from the definition of the inner products associated with the Fourier transform defined by (2), the matrix elements are

$$K_{im}^{(1,1)}(k_0) = \sum_{n=1}^{\infty}\int_0^{\infty} \tilde{J}_{zi}(n,\beta)\tilde{G}_{11}(n,\beta,k_0)\tilde{J}_{xm}(n,\beta)\, d\beta \tag{15a}$$

$$K_{im}^{(1,2)}(k_0) = \sum_{n=1}^{\infty}\int_0^{\infty} \tilde{J}_{zi}(n,\beta)\tilde{G}_{12}(n,\beta,k_0)\tilde{J}_{zm}(n,\beta)\, d\beta \tag{15b}$$

$$K_{im}^{(2,1)}(k_0) = \sum_{n=1}^{\infty}\int_0^{\infty} \tilde{J}_{xi}(n,\beta)\tilde{G}_{21}(n,\beta,k_0)\tilde{J}_{xm}(n,\beta)\, d\beta \tag{15c}$$

$$K_{im}^{(2,2)}(k_0) = \sum_{n=1}^{\infty}\int_0^{\infty} \tilde{J}_{xi}(n,\beta)\tilde{G}_{22}(n,\beta,k_0)\tilde{J}_{zm}(n,\beta)\, d\beta. \tag{15d}$$

The right-hand sides of (10) can be eliminated in Galerkin's process via the application of Parseval's relation, because the inverse transforms of $\tilde{E}_x$, $\tilde{E}_z$ and $\tilde{J}_x$, $\tilde{J}_z$, i.e., E_x, E_z and J_x, J_z, are nonzero only in the complementary regions in the (x,z) plane at $y = d$.

The simultaneous equations (14) are now solved for the wavenumber k_0 by setting the determinant of the coefficient matrix equal to zero and by seeking the root of the resulting characteristic equation. The resonant frequency of the microstrip resonator shown in Fig. 1 is derived from the obtained value of k_0.

The accuracy of the solution can be systematically improved by increasing the number of basis functions $(M + N)$ and by solving larger size matrix equations. However, if the first few basis functions are chosen so as to approximate the actual unknown current distribution reasonably well, the necessary size of the matrix can be held small for a given accuracy of the solution, resulting in the numerical efficiency. Hence the choice of basis functions is important from the numerical point of view.

In actual computations for the dominant mode, $\tilde{J}_{z1}$ and $\tilde{J}_{x1}$ have been chosen to be

$$\tilde{J}_{z1}(n,\beta) = \tilde{J}_1(n)\tilde{J}_2(\beta) \tag{16a}$$

$$\tilde{J}_{x1}(n,\beta) = \tilde{J}_3(n)\tilde{J}_4(\beta) \tag{16b}$$

where

$$\tilde{J}_1(n) = \frac{2\sin(\hat{k}_n w)}{\hat{k}_n w} + \frac{3}{(\hat{k}_n w)^2}\left\{\cos(\hat{k}_n w) - \frac{2\sin(\hat{k}_n w)}{\hat{k}_n w} + \frac{2[1-\cos(\hat{k}_n w)]}{(\hat{k}_n w)^2}\right\}$$

$$\tilde{J}_2(\beta) = \frac{-\pi\cos(\beta l)}{(\beta l)^2 - (\pi/2)^2}$$

$$\tilde{J}_3(n) = \frac{2\pi\sin(\hat{k}_n w)}{(\hat{k}_n w)^2 - \pi^2}$$

$$\tilde{J}_4(n) = \frac{\cos(\beta l)}{\beta l} - \frac{\sin(\beta l)}{(\beta l)^2}.$$

Note that (16) are the Fourier transforms of $J_{z1}(x,z) = J_1(x)J_2(z)$ and $J_{x1}(x,z) = J_3(x)J_4(z)$ where the functional forms of J_1–J_4 are given in Fig. 2. Higher order $\tilde{J}_{zm}$ and $\tilde{J}_{xm}$ may be chosen in a similar manner. It may be worthwhile to mention that the form of $\tilde{J}_1$ is identical to the one used by Denlinger [11] for computing the dispersion characteristics of infinitely long microstrip lines.

It must be pointed out that, although the numerical computations carried out in this paper are for the dominant resonance mode only, the method developed in this paper is equally well applicable to the higher order modes. For computing such higher order resonances, it is only necessary to use the basis functions appropriate for the specific mode of interest. For instance, for the resonance of the second order in the z direction, $\cos(\pi z/l)/l$ may be used instead of J_2 shown in Fig. 2.

Before ending this section, some of the unique features of the present method will be summarized.

1) The spectral method is numerically simpler and more efficient than many space-domain methods, primarily because in the present method solutions are extracted from algebraic equations rather than from coupled integral equations of convolution type. Furthermore, the Fourier transforms of Green's functions $\tilde{G}_{11}$, $\tilde{G}_{12}$, $\tilde{G}_{21}$, and $\tilde{G}_{22}$ in (10) have simple closed forms. On the other hand, in the space-domain methods, the Green's functions are inverse Fourier transforms of $\tilde{G}_{11}$, etc., and hence are numerically much more difficult to evaluate [12]. For instance

$$\tilde{G}_{11}(x-x',y,y',z-z')\,|_{y=y'=d} = \frac{2}{\pi a}\sum_{n=1}^{\infty}\exp(-j\hat{k}_n\,|\,x-x'\,|) \cdot \int_0^{\infty} G_{11}(n,\beta)\exp(-j\beta\,|\,z-z'\,|)\,d\beta.$$

2) Although numerical computation of $K_{im}^{(1,1)}$, etc., requires the evaluation of the infinite summations of infinite integrals, as shown in (15), they can be efficiently obtained after truncating these infinite summations and integrals at some finite points, because the integrands in (15) decrease quickly. For instance, for $\tilde{J}_{z1}$ and $\tilde{J}_{x1}$ in (16), they decay as fast as $(\hat{k}_n w)^{-3}$ and $(\beta l)^{-3}$.

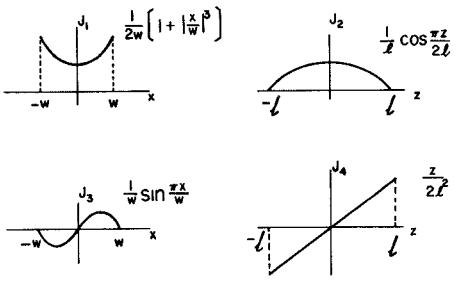

Fig. 2. Forms of assumed current distributions.

3) As pointed out earlier, the solution in the present method can be systematically improved by increasing the number of basis functions and solving a larger size matrix.

4) The physical nature of the field corresponding to each mode is directly incorporated in the process of solution via the appropriate choice of basis functions.

III. RESULTS AND DISCUSSIONS

Before presenting the numerical results and experimental data, it should be noted that the structures used for both numerical computations and experiments throughout the rest of this paper are scale models of millimeter-wave integrated circuits. In practice, after the circuit is designed and tested at low frequencies, a miniature structure for millimeter-wave integrated circuits may be obtained by reducing all the dimensions of the circuit structure while keeping the ratios of all the dimensions to the wavelength constant. The value of the relative dielectric constant of the substrate is assumed to be unchanged in these two frequency ranges. Since the field distributions in both the scale models and the actual millimeter-wave circuits constructed in this manner are the same, we are solving the field problem of millimeter-wave integrated circuit structures even though the actual operating frequencies are in the UHF range.

Numerical computations have been carried out for the resonant frequencies of microstrip resonators using a CDC G-20 computer which is about ten times slower than the IBM 360/75. Each matrix element in (14) such as $K_{im}^{(1,1)}$ has been computed accurately up to five significant digits or better. To test the convergence of the present method, the resonant frequency has been calculated for two choices of matrix size: 1) $N = 1$, $M = 0$; 2) $N = M = 1$. In case 1), only the axial component J_{z1} of the resonator current is retained. Fig. 3 shows some typical results obtained by choices 1) and 2). It is clear that the two sets of values are very close except for very wide resonators in which the J_x component is physically expected to make more significant contributions. Some test calculations that include higher order basis functions

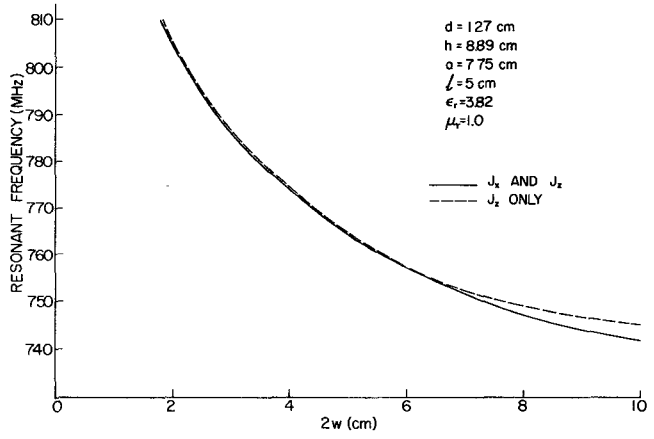

Fig. 3. Comparison of resonant frequencies derived from $N = 1$, $M = 0$, and $N = M = 1$ cases.

TABLE I
RESONANT FREQUENCY VERSUS LOADED Q ($2l$ = 10-CM RESONATOR)

Loaded Q	Resonant Frequency (MHz)
37	708.0
106	730.6
466	742.3
688	743.0
1509	746.0
1735	746.4
2334	747.0
10000	753.0*
Present theory	752.4

Note: * is the extrapolated value.

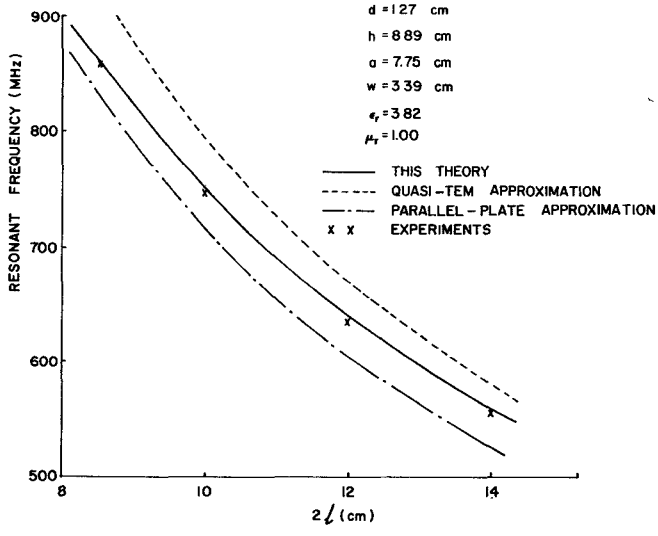

Fig. 4. Comparison of the results from the present methods with those obtained from experiments and other methods.

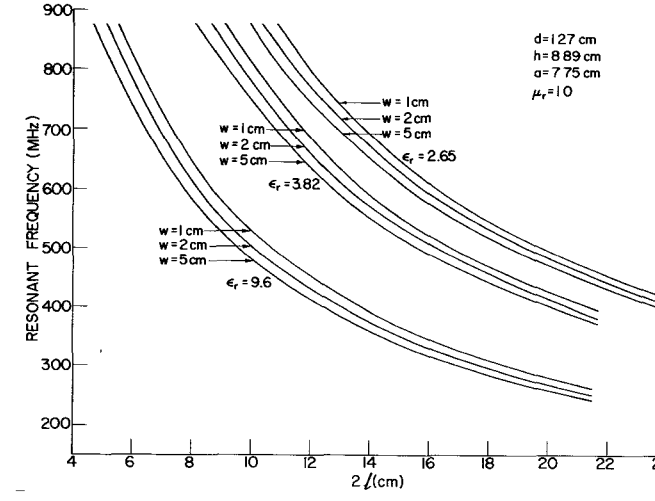

Fig. 5. Resonant frequencies of microstrip resonators with various structural parameters.

($N = M = 2$) gave so small a difference from the $N = M = 1$ case that the results were almost indistinguishable on the graphical figures. In the rest of this paper only the results from the $N = M = 1$ case will be used.

Fig. 4 shows the resonant frequency versus the length of the resonator. Other theoretical results are based on the open-ended quasi-TEM as well as the parallel-plate transmission line models. The latter is of width $2w$ and thickness d, has magnetic side walls, and is filled with a medium of dielectric constant ϵ_r. In both of these approximation models, the resonant frequency was computed from the length of $2(l + \Delta l)$ where $\Delta l = 0.3d$ is the hypothetical extension of the line to account for the end effect [7].

The experiments[1] have been conducted using the strip of thickness 0.254 mm that is negligibly small compared to other dimensions. The loaded Q of the resonant circuit was maintained around 1450. As seen from Fig. 4, the agreement between the experimental data and the results computed by the present theory is extremely good. In order to study the effect of the loaded Q of the circuit on the resonant frequency measurement, one of the resonators used in Fig. 4 was loaded differently and the resonant frequency was measured as a function of loaded Q. The results summarized in Table I show that the numerical results are even closer to the resonant frequency of an extremely loosely coupled resonator—in fact, the frequency of an essentially uncoupled resonator.

Fig. 5 shows the resonant frequencies of microstrip resonators with various structural parameters. As expected, the resonant frequency is lower for the resonator of the same dimension but with the substrate of higher dielectric constant.

Finally, the typical computation time using the $N = M = 1$ case was about 200 s/structure although the time is longer for narrower resonators.

IV. END EFFECT

To date, the end effect of the open-ended microstrip lines has been studied with the quasi-static approximation [5]–[7]. However, at higher frequencies, say millimeter-wave regions, the quasi-static approximation may not be

[1] The author would like to thank W. W. Snell, Jr., of Bell Laboratories, Holmdel, New Jersey, for furnishing the experimental data.

accurate. In this section, the resonant frequency data of the microstrip resonators have been used for estimating the end effect at the open ends of microstrip lines using the full-wave theory.

First, compute the dispersion characteristics [13], [14] of the infinitely long microstrip line with the same cross-sectional structure as the microstrip resonator. From the dispersion relation the guide wavelength λ_g is derived at the resonant frequency f_c of the microstrip resonator of length $2l$.

Now, consider the hypothetical open-circuited microstrip resonator whose structure is identical to Fig. 1 except that the length is $2\bar{l}$ instead of $2l$. The hypothetical length $2\bar{l}$ is determined from the resonant condition of the open-circuited line $2\bar{l} = \lambda g/2$. The hypothetical extension of the microstrip line, which accounts for the end effect, is given by $\Delta l = \bar{l} - l$.

Fig. 6 shows that the values of Δl are considerably smaller than those computed by the quasi-static approximation. It is conjectured that these smaller values may be caused by the reduction of the capacitive susceptance due to the lumped inductance associated with the disturbance in the current components at the strip ends. Fig. 7 shows that when the length l is increased, Δl first decreases because of the decrease of mutual coupling between two ends. However, when l is further increased, Δl increases. This phenomenon occurs probably because for large l the resonant frequency decreases and hence the situation approaches the static limit where the Δl value is much larger, as shown in Fig. 6.

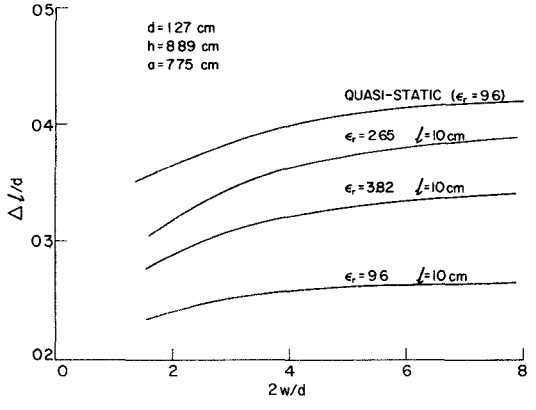

Fig. 6. End effect versus the width of strip.

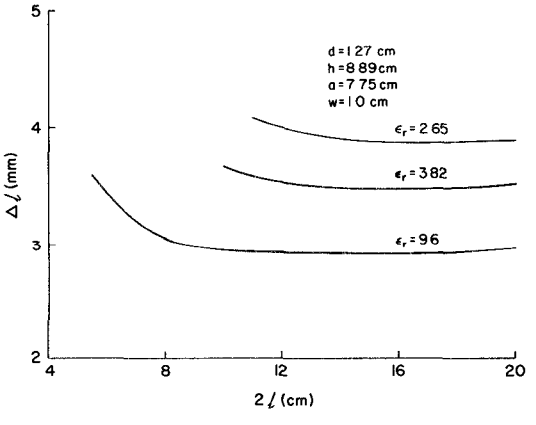

Fig. 7. End effect versus the length of strip.

V. CONCLUSION

A new efficient method has been developed for computing the resonant frequencies of rectangular microstrip resonators. The formulation is based on the rigorous full-wave analysis. The characteristic equation has been obtained via the application of Galerkin's method in the spectral domain. The numerical results were compared with those derived from other theoretical and experimental data. The agreement between the experimental results and the data computed from the present method was extremely good.

Further, the results for microstrip resonators have been used for estimating the end effect of the microstrip lines. The estimate has been compared with the values obtained by the quasi-static theory.

Finally, it should be mentioned that the operating frequency in the paper was assumed to be below cutoff of the shielding waveguide. When this is no longer the case, all the formulas given in this paper still hold. However, in such situations the "det" in (11d) possesses zeros on the real axis in the complex β plane. Hence because of the poles of $\tilde{G}_{11}$, etc., the matrix elements $K_{im}^{(1,1)}$, etc., now become complex, and the characteristic equation for the resonant frequency is satisfied only with the complex k_0. Physically, this situation corresponds to the finite value of resonator Q due to the coupling to the waveguide modes.

It is planned in the future to obtain more data for various structural parameters and to extend the present method to the case where the shielding walls are removed or the operating frequency is above waveguide cutoff.

ACKNOWLEDGMENT

The author wishes to thank Prof. J. D. Dyson and Prof. R. Mittra for their useful comments.

REFERENCES

[1] M. V. Schneider, "Millimeter-wave integrated circuits," presented at the IEEE G-MTT Int. Symp. Microwaves, Boulder, Colo., June 1973.
[2] S. Mao, S. Jones, and G. D. Vendelin, "Millimeter-wave integrated circuits," *IEEE Trans. Microwave Theory Tech. (Special Issue on Microwave Integrated Circuits)*, vol. MTT-16, pp. 455–461, July 1968.
[3] T. Itoh and R. Mittra, "Analysis of a microstrip disk resonator," *Arch. Elek. Übertragung.*, vol. 27, pp. 456–458, Nov. 1973.
[4] J. Wolff, and N. Knoppik, "Rectangular and circular microstrip disc capacitors and resonators," presented at the European Microwave Conf., Brussels, Belgium, Sept. 1973, Paper B.4.1.
[5] P. Silvester and P. Benedek, "Equivalent capacitance of microstrip open circuits," *IEEE Trans. Microwave Theory Tech.*, vol. MTT-20, pp. 511–516, Aug. 1972.
[6] A. Farrar and A. T. Adams, "Matrix method for microstrip three-dimensional problems," *IEEE Trans. Microwave Theory Tech.*, vol. MTT-20, pp. 497–604, Aug. 1972.
[7] T. Itoh, R. Mittra, and R. D. Ward, "A method for computing edge capacitance of finite and semi-infinite microstrip lines," *IEEE Trans. Microwave Theory Tech.* (Short Papers), vol. MTT-20, pp. 847–849, Dec. 1972.
[8] T. Itoh and R. Mittra, "A new method for calculating the capacitance of a circular disk for microwave integrated circuits," *IEEE Trans. Microwave Theory Tech.* (Short Papers), vol. MTT-21, pp. 431–432, June 1973.
[9] ——, "Spectral-domain approach for calculating the dispersion characteristics of microstrip lines," *IEEE Trans. Microwave Theory Tech.* (Short Papers), vol. MTT-21, pp. 496–499, July 1973.

[10] C. C. Kao, "Three-dimensional electromagnetic scattering from a circular tube of finite length," *J. Appl. Phys.*, vol. 60, pp. 4732–4740, Nov. 1969.
[11] E. J. Denlinger, "A frequency dependent solution for microstrip transmission lines," *IEEE Trans. Microwave Theory Tech.*, vol. MTT-19, pp. 30–39, Jan. 1971.
[12] E. Yamashita and K. Atsuki, "Strip line with rectangular outer conductor and three dielectric layers," *IEEE Trans. Microwave Theory Tech.*, vol. MTT-18, pp. 238–244, May 1970.
[13] R. Mittra and T. Itoh, "A new technique for the analysis of the dispersion characteristics of microstrip lines," *IEEE Trans. Microwave Theory Tech.*, vol. MTT-19, pp. 47–56, Jan. 1971.
[14] T. Itoh and R. Mittra, "A technique for computing dispersion characteristics of shielded microstrip lines," *IEEE Trans. Microwave Theory Tech.* (Short Papers), vol. MTT-22, pp. 896–898, Oct. 1974.

Short Papers

Analysis of Lossy Inhomogeneous Waveguides Using Shooting Methods

R. E. McINTOSH, SENIOR MEMBER, IEEE, AND L. J. TURGEON, STUDENT MEMBER, IEEE

Abstract—**Shooting methods are used to analyze rectangular waveguides containing inhomogeneous lossy dielectrics. The technique obtains the electromagnetic fields inside the waveguide by solving Maxwell's equations using trial and error procedures to match the boundary conditions at the conducting waveguide surface. Dispersion and attenuation curves are obtained which show how continuous dielectric inhomogeneities and losses affect the transmission characteristics of these waveguides.**

I. INTRODUCTION

The many applications of inhomogeneously loaded waveguides in microwave engineering has resulted in a need for methods of calculating the transmission characteristics of the waves that propagate in such waveguides. A number of solution methods have been developed to analyze such problems, most of which are numerical, since only a few inhomogeneous cases can be solved in closed form [1].

Most of the methods developed are restricted to lossless inhomogeneities. Some of the earlier ones [2]–[4] treat waveguides containing one or two slabs of lossless dielectric. Further developments include Galerkin's method and modification thereof [5], [6], analytical approximations [7], Rayleigh–Ritz optimization [8], [1], finite difference [9], finite element (especially helpful for arbitrary waveguide cross sections) [10]–[12], computer iterations [13], vector variational [14], and shooting methods [15].

Rectangular waveguides containing lossy dielectric slabs have also been analyzed [13], [16]–[18]. Perhaps one of the more elegant papers in this area was written by Gardiol [18]. Using a matrix formulation, he treated general waveguides containing linear, inhomogeneous, lossy, and anisotropic slabs. In principle, his formulation is valid for solving waveguides which have any number of slabs extending across them. However, in practice, the number of computer operations prohibits the computation of waveguide propagation constants (even for the isotropic case) when a large number (e.g., more than 25) of slabs are needed to model the medium contained inside the waveguide. This limitation is not very important in those situations where the medium is accurately modeled by a few step discontinuities but it can be serious when treating certain geometries with continuously varying media.

Manuscript received August 8, 1973; revised June 10, 1974. This work was supported in part by the Air Force Office of Scientific Research under Grant AFOSR 69–1722.
The authors are with the Wave Propagation Laboratory, Department of Electrical and Computer Engineering, University of Massachusetts, Amherst, Mass. 01002.

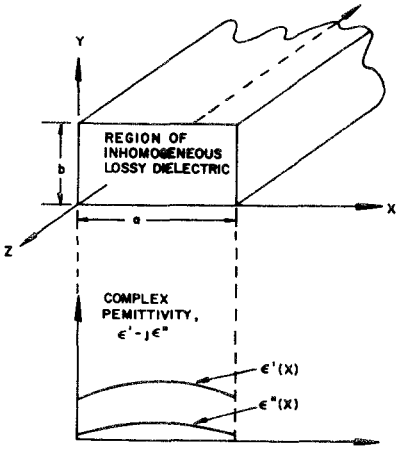

Fig. 1. Rectangular inhomogeneous lossy waveguide with width a and height b. The permittivity $\epsilon(x) = \epsilon'(x) - j\epsilon''(x)$ is a function of the spatial coordinate x.

In this short paper we present an approach which differs from Gardiol's in the technique used to solve Maxwell's equations. We show that the propagation characteristics of a rectangular waveguide loaded with an isotropic, lossy, and inhomogeneous dielectric as shown in Fig. 1 can be found by applying shooting methods directly to the field equations. This technique has the advantage that the permittivity does not have to be approximated by a small number of slabs. The field components are also available for printout and display since they are computed in determining the dispersion curves.

The complex propagation constants for an inhomogeneous rectangular waveguide are obtained by solving the first-order differential equations (Maxwell's equations) using Hammings stable method [19], started by a Runge–Kutta–Gill method. The ability to select the size of the spatial increments used in the iteration procedure further allows this technique to yield good accuracy for higher order modes and strong inhomogeneities of the permittivity [15].

In Section II, Maxwell's equations are formulated appropriately for a rectangular geometry, and a description of the solution technique is given when the inhomogeneity can be expressed as a function of one spatial coordinate. An example is presented in Section III to illustrate the speed and accuracy of the method.

II. THEORY

Maxwell's equations contain all of the necessary information to obtain the wave propagating characteristics of waveguides. We need only solve them inside the waveguide of width a and height b shown in Fig. 1 subject to the appropriate boundary conditions. For one-dimensional inhomogeneities in the x direction, the electric field